

Quantum chemical study of the Fe(III)-desferrioxamine B siderophore complex—Electronic structure, vibrational frequencies, and equilibrium Fe-isotope fractionation

S.D. Domagal-Goldman^{a,*}, K.W. Paul^b, D.L. Sparks^c, J.D. Kubicki^{a,d}

^a Department of Geosciences, The Pennsylvania State University, University Park, PA 16802, USA

^b U.S. Army Research Laboratory, AMSRD-ARL-WM-BD, Aberdeen Proving Ground, MD 21005, USA

^c Department of Plant and Soil Sciences, University of Delaware, Newark, DE 19717-1303, USA

^d The Earth & Environmental Systems Institute, The Pennsylvania State University, University Park, PA 16802, USA

Received 30 July 2007; accepted in revised form 19 September 2008; available online 17 October 2008

Abstract

This study presents molecular orbital/density functional theory (MO/DFT) calculations of the electronic structure, vibrational frequencies, and equilibrium isotope fractionation factors for iron desferrioxamine B (Fe-DFO-B) complexes in aqueous solution. In general, there was good agreement between the predicted properties of Fe(III)-DFO-B and previously published experimental and theoretical results. The predicted fractionation factor for equilibrium between Fe(III)-DFO-B and Fe(III)-catecholate at 22 °C, $0.68 \pm 0.25\text{‰}$, was in good agreement with a previously measured isotopic difference between bacterial cells and solution during the bacterial-mediated dissolution of hornblende [Brantley S. L., Liermann L. and Bullen T. D. (2001) Fractionation of Fe isotopes by soil microbes and organic acids. *Geology* **29**, 535–538]. Conceptually, this agreement is consistent with the notion that Fe is first removed from mineral surfaces via complexation with small organic acids (e.g., oxalate), subsequently sequestered by DFO-B in solution, and ultimately delivered to bacterial cells by Fe(III)-DFO-B complexes. The ability of DFO-B to discriminate between Fe(III) and Fe(II)/Al(III) was investigated with Natural Bond Orbital (NBO) analysis and geometry calculations of each metal-DFO-B complex. The results indicated that higher affinity for Fe(III) is not strictly a function of bond length but also the degree of Fe–O covalent bonding.

© 2008 Elsevier Ltd. All rights reserved.

1. INTRODUCTION

Iron is an essential nutrient for the majority of organisms and functions in a variety of cell reduction and enzymatic processes. Despite the high natural abundance of iron, its availability to plants and microorganisms under aerobic, neutral pH conditions is limited. Iron limitations primarily arise from the low solubility of Fe(III), which at circumneutral pH is $\sim 10^{-18}$ M with respect to most Fe(III)-bearing minerals (Kiss and Farkas, 1998). Because

of the difference between the biological demand for Fe and its availability, accumulation of Fe by organisms significantly impacts its cycling in natural systems and Fe can be a limiting factor for biological productivity (Martin and Fitzwater, 1988).

Siderophores, an important class of organic acids with large complexation constants for Fe, are produced by several organisms in order to overcome iron deficiencies (Wiederhold et al., 2006). Due to their exceptionally high affinity for Fe, siderophores complex Fe(III) by extracting it from Fe-bearing minerals or aqueous Fe(III) complexes. Fe-siderophore complexes can then be delivered to an organism for uptake through a variety of cellular recognition and transport mechanisms (Albrecht-Gary and Crumbliss, 1998; Boukhalfa and Crumbliss, 2002). Subsequent release

* Corresponding author. Present address: Astronomy Department, University of Washington, Seattle, WA 98195, USA.

E-mail address: sgoldman@astro.washington.edu (S.D. Domagal-Goldman).

of Fe, at or through an organism's cell membrane, allows the siderophore to scavenge for additional Fe.

Complexation of Fe(III) by naturally synthesized siderophores is efficient because of the remarkably large association constants for Fe(III)–siderophore complexes. Association constants for Fe(III)–siderophore complexes range between 10^{23} to 10^{52} (Hernlem et al., 1996; Albrecht-Gary and Crumbliss, 1998). Chemical specificity for Fe(III) is readily achieved because association constants between siderophores and other di- and tri-valent metals are relatively smaller. For example, the association constants for desferrioxamine B (DFO-B) (a natural siderophore synthesized by the soil actinomycete *Streptomyces pilosus*) with different metals are as follows: Fe(III) = $10^{42.33}$, Ga(III) = $10^{38.96}$, Al(III) = $10^{36.11}$, Ni(II) = $10^{27.66}$, Cu(II) = $10^{23.98}$, and Zn(II) = $10^{20.40}$ (Anderegg et al., 1963; Evers et al., 1989; Kurzak et al., 1992; Hernlem et al., 1996). This chemical specificity is important in environments such as soils, where Al(III) concentrations may be comparable to Fe(III) concentrations. Because Al(III) is phytotoxic (Kochian, 1995, and references therein), the ability to uptake Fe(III) and exclude Al(III) is critical to plant health.

Cheah et al. (2003) reported that the dissolution of goethite in the presence of both oxalate and DFO-B was enhanced relative to experiments involving just one of these two organic acids; the authors suggested that Fe transport from a mineral surface to a bacterial cell involves a concerted multi-step process. First, oxalate extracts Fe from the mineral surface and Fe-oxalate complexes diffuse into solution. Second, DFO-B scavenges Fe from Fe-oxalate complexes, freeing oxalate to return to the mineral surface. Finally, Fe-DFO-B complexes transport Fe to bacterial cells and release of Fe allows DFO-B to scavenge additional Fe.

Other studies have measured the fractionation of Fe isotopes during leaching of Fe from hornblende (Brantley et al., 2001) and goethite (Brantley et al., 2004). The former of those two studies reported that the amount of Fe isotope fractionation between hornblende and solution depended on the Fe-ligand affinity. That study also noted an isotopic fractionation between Fe that remained in solution and Fe that was incorporated into bacterial cells (0.85 and $1.17 \pm 0.20\text{‰}$). In these isotope studies, a major challenge was quantifying and discriminating between the amount of fractionation caused by equilibrium effects in solution and by kinetic effects at mineral-solution and solution-cell interfaces. The first measurements of fractionations between organic-bound and inorganic Fe in solution recently appeared in the literature (Dideriksen et al., 2008), and this study aims to re-produce the fractionations reported in that study.

The process of separating ligand-bound Fe from aqueous Fe can lead to isotopic fractionation (Wiederhold et al., 2006). Thus, validation and interpretation of experimental findings would be greatly assisted by the development of models that can accurately predict isotope fractionation factors. Isotope fractionation factors have already been predicted and measured for Fe(II)–(H₂O)₆ and Fe(III)–(H₂O)₆ (Johnson et al., 2002; Welch et al., 2003; Jarzecki et al., 2004; Anbar et al., 2005; Domagal-Goldman

and Kubicki, 2008), and have been predicted for Fe(II)-oxalate and Fe(III)-oxalate (Domagal-Goldman and Kubicki, 2008). However, fractionation factors for siderophore complexes have not been previously predicted.

The objectives of this study were to examine the high affinity and specificity of DFO-B for Fe(III) and to predict the equilibrium Fe isotope fractionations associated with the Fe-DFO-B complex in solution. First, we present the effects of different methodologies on the predicted structure of DFO-B complexes because Fe–O bond distances influence both Fe isotope fractionation factors and Fe affinities. We then examine the chemical specificity for Fe using NBO (Natural Bond Orbital) analysis (Weinhold and Landis, 2001) of Fe(III)-DFO-B, Fe(II)-DFO-B, and Al(III)-DFO-B, whereby the electron occupancies of Fe–O/Al–O bonds and the partial charges of the Fe/Al atoms are predicted. We also present predicted vibrational frequencies for Fe(III)-DFO-B and Fe(II)-DFO-B complexes, since these predictions affect the accuracy of calculated equilibrium isotope constants for Fe(III)-DFO-B and Fe(II)-DFO-B.

2. METHODS

2.1. Complexes studied

The siderophore examined in this study was DFO-B, the most extensively studied siderophore with respect to mineral dissolution of the approximately 500 known siderophore structures (Wiederhold et al., 2006). DFO-B is a linear trihydroxamic acid composed of 1,5-diaminopentane and succinic acid residues. DFO-B has four acidic protons (three hydroxamic acids and one terminal amine), is positively charged, and is soluble in water and alcohols (Borgias et al., 1989). DFO-B coordinates Fe(III) through six oxygen donors, forming three chelate rings in a distorted octahedral symmetry. The resulting Fe(III)-DFO-B hexadentate complex has 16 possible geometrical and optical isomers that have small energy differences (Leong and Raymond, 1975; Borgias et al., 1989; Dhungana et al., 2001).

Previous investigations of hydroxamate complexes at the goethite-water interface have been conducted. Holmen and coworkers (Holmen and Casey, 1996; Holmen et al., 1997) used acetohydroxamic acid (aHa) as an analog for high molecular weight hydroxamate siderophores and performed Hartree–Fock calculations to investigate various conformations of aHa. Edwards et al. (2005) used the B3LYP/6-311G(d) method to predict the vibrational frequencies of Fe–aHa complexes. To date, isotope fractionation factors have not been predicted for Fe-DFO-B. Under circumneutral pH conditions, Fe(III)-DFO-B has a +1 charge arising from the terminal amine group. However, in the crystal structure, the +1 charge is balanced by a counter-ion. For the gas-phase calculations, we used a neutrally charged Fe(III)-DFO-B complex in order to minimize intra-molecular H-bonding interactions that do not exist in solution (Section 3.2). For the solution-phase calculations, we used the protonated Fe(III)-DFO-B complex because inclusion of solvation prevented the formation of artificial intra-molecular H-bonds (Fig. 1).

2.2. Quantum chemical calculations

Molecular orbital/density functional theory (MO/DFT) calculations were performed with Gaussian 03 (Frisch et al., 2004). Specifically, we employed the unrestricted B3LYP method, comprised of Becke's (Stephens et al., 1994; Becke, 1997) 3-parameter nonlocal-exchange functional (B3), and Lee, Yang, and Parr's (Lee et al., 1988) gradient-corrected correlation functional (LYP). The B3LYP method has been shown to accurately predict the molecular structures and vibrational frequencies of transition metal complexes (Koch and Holthausen, 2001), including Fe-aHa and an analog for DFO-B (Edwards et al., 2005).

The local bonding environment of Fe(III)-DFO-B, as predicted by the MO/DFT calculations, was compared to experimental single-crystal X-ray diffraction data (Dhungana et al., 2001) and EXAFS measurements of the solvated complex (Edwards and Myneni, 2005). MO/DFT predictions are presented with the following basis sets: 6-31G,

6-31G(d), 6-31+G(d), 6-311G(d), 6-311G(d,p), and 6-311+G(d). The geometries were predicted from energy minimizations performed without symmetry constraints that could have potentially biased the predictions. Frequency calculations were subsequently performed to verify that a minimum-energy structure was located (i.e., no imaginary frequencies).

IR frequencies are reported for gas-phase Fe(III)-DFO-B and Fe(II)-DFO-B complexes, using the B3LYP/6-311G(d,p) method. A similar method (B3LYP/6-311G(d)) accurately predicted the IR frequencies for Fe(III)-triscatechol and Fe(III)-trisoxalate, two complexes with octahedral coordination similar to Fe(III)-DFO-B (Domagal-Goldman and Kubicki, 2008). Frequencies were scaled by a factor of 0.956 in order to account for errors associated with the use of a harmonic oscillator approximation (Hehre et al., 1985) as well as the inaccuracies associated with the DFT method. This scale factor was developed via modeling of smaller Fe-organic complexes (Edwards et al., 2005), has

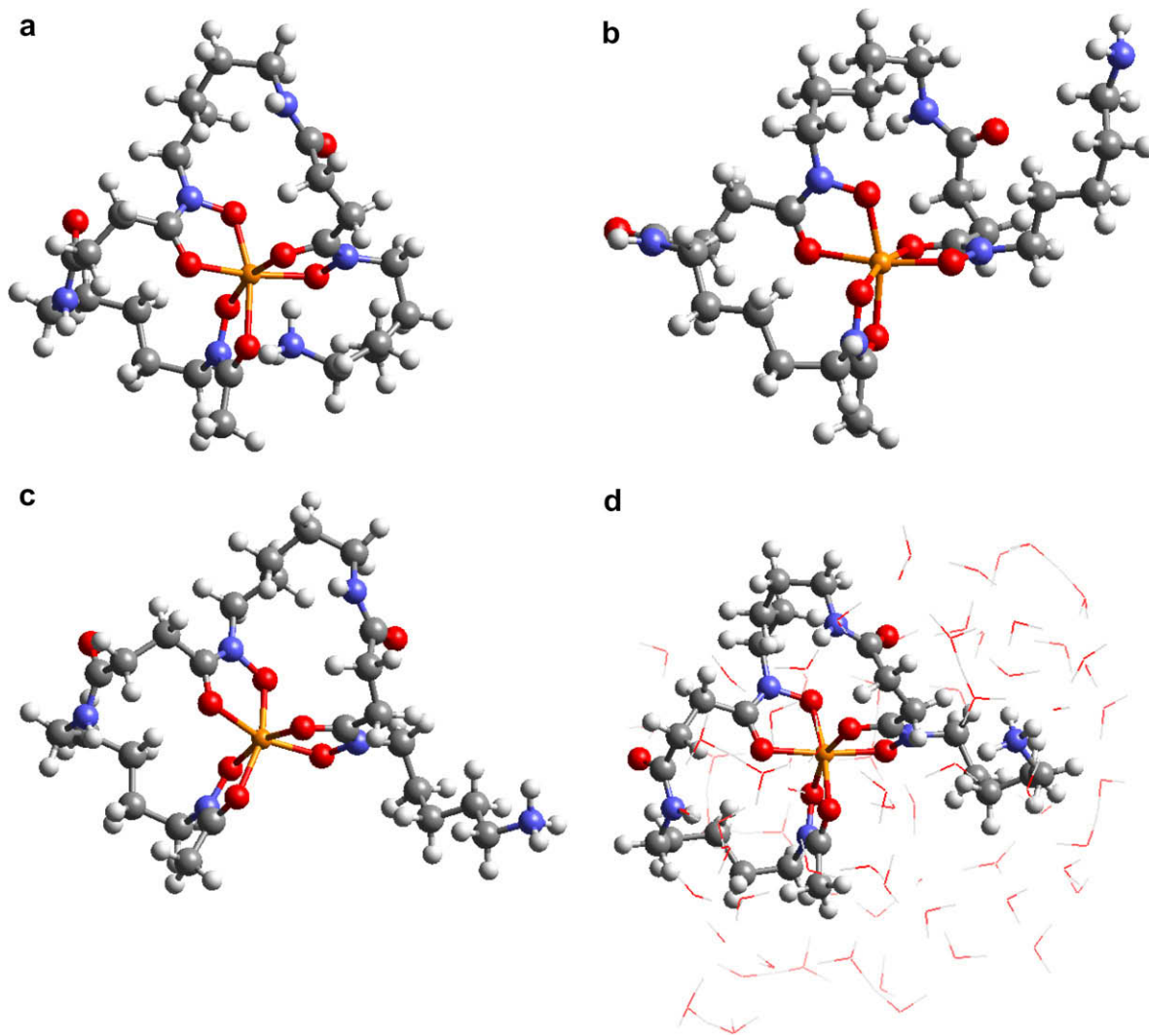


Fig. 1. Optimized geometries for protonated gas-phase Fe-DFO-B (a); de-protonated gas-phase Fe-DFO-B (b); protonated Fe-DFO-B in solution using IEFPCM (c); and protonated Fe-DFO-B in solution using 72 explicit H₂O molecules (d).

proven effective for modeling the IR frequencies of other Fe-organic complexes (Domagal-Goldman and Kubicki, 2008), and its use in this study slightly reduced the disagreement between predicted and measured IR frequencies.

The Integral Equation Formalism Polarizable Continuum Model (IEFPCM, Cancès et al., 1997) was used to account for solvation implicitly. When using IEFPCM, the large size of the siderophore and corresponding complexity of the solvation cavity caused difficulties with energy minimizations. These difficulties were alleviated by using a smaller basis set (6-31G instead of 6-311G(d,p)) and by decreasing the number of spheres used to create the IEFPCM cavity. The latter modification was accomplished by increasing the minimum radii of the spheres from 0.2 Å to 0.5 Å and reducing the default overlap index in Gaussian 03 (Frisch et al., 2004) from 0.89 to 0.8.

Explicit solvation was also used to model the Fe(III)-DFO-B complex in a water droplet composed of 72 H₂O molecules. After an initial “water droplet” structure was obtained from a force-field based energy minimization in Cerius² (Accelrys, 2003), a DFT energy minimization of the complex was performed using the CEP-121G (Walker et al., 1983; Cundari and Stevens, 1993) basis set for Fe, and the 3-21G(d,p) basis set for the remaining atoms. A larger basis set for the C, N, O, and H atoms was impractical considering the system size and availability of computational resources.

To examine the contributions of covalent bonding to the high chemical specificity for Fe by DFO-B, the orbital occupancies of Fe(II)-, Fe(III)-, and Al(III)-DFO-B were calculated using NBO analysis. Single-point NBO calculations were performed using the B3LYP/6-311++G(d,p) method and the NBO 3.0 utility (Foster and Weinhold, 1980; Reed and Weinhold, 1983; Reed et al., 1985, 1988; Carpenter and Weinhold, 1988) included with Gaussian 03. The single-point NBO calculations were performed on the B3LYP/6-311G(d) energy-minimized geometries.

2.3. Calculation of isotope fractionation factors

Equilibrium isotope fractionation factors were calculated from the predicted vibrational frequencies of the Fe-DFO-B complexes (⁵⁶Fe and ⁵⁴Fe), according to the equa-

tions of Urey (1947). First, we predicted the equilibrium constants for isotope exchange between a complex and a reservoir of the isotopically active element. This constant is represented by β and is given by the ratio of the partition function with isotope A (Q_A) to the partition function with isotope B (Q_B):

$$\beta = \frac{Q_A}{Q_B} = \prod_i \left(\frac{\nu_{Ai}}{\nu_{Bi}} \frac{e^{-h\nu_{Ai}/2kT}}{1 - e^{-h\nu_{Ai}/kT}} \frac{1 - e^{-h\nu_{Bi}/kT}}{e^{-h\nu_{Bi}/2kT}} \right), \quad (1)$$

where the product is taken over the 3N-6 vibrational modes (ν_i), N is the number of atoms in the complex, k is the Boltzmann constant, and T is temperature. In this study, fractionation was predicted for the two most common isotopes of Fe, ⁵⁶Fe and ⁵⁴Fe ($A = 56$ and $B = 54$). This form of Eq. (1) utilizes the ratio of vibrational frequencies (Redlich, 1935) to convert β into a reduced partition function. The use of this form of the equation is critical when using implicit solvation techniques (Domagal-Goldman and Kubicki, 2008) and has been shown to lead to smaller error propagation from inaccurate frequency predictions (Schaad, 1999). Once β was calculated, the equilibrium fractionation factor, α , was calculated from the ratio of β values for the two complexes. α (and by association, β) are useful in predicting equilibrium fractionations according to the following equation:

$$\begin{aligned} \Delta^{56}\text{Fe}(X - Y) &\approx 1000 \cdot \ln(\alpha_{X-Y}) \\ &= 1000 \cdot [\ln(\beta_X) - \ln(\beta_Y)]. \end{aligned} \quad (2)$$

3. RESULTS AND DISCUSSION

3.1. Basis set effects: local bonding structure

In Table 1, the structure of the energy-minimized gas-phase Fe(III)-DFO-B complex is compared to both experimental single-crystal X-ray diffraction data (Dhungana et al., 2001) and solution EXAFS measurements (Edwards and Myneni, 2005). When compared to the single-crystal X-ray diffraction data, the MO/DFT predictions overestimated the Fe–O(C) bond lengths by 0.06–0.08 Å and underestimated the Fe–O(N) bond lengths by about 0.02 Å. The average Fe–O bond lengths compared well to

Table 1

Fe(III)-DFO-B structure based upon single-crystal X-ray diffraction measurements (a—Dhungana et al., 2001), EXAFS measurements of the Fe-DFO-B complex in solution (b—Edwards et al., 2005), and gas-phase MO/DFT predictions (this study). The MO/DFT predictions are labeled by the basis set. Fe–O(C) and Fe–O(N) represent Fe–O bond lengths, where the O atom is bound to a C or N atom. All values are averaged (Å for bond lengths and ° for angles).

Fe(III)-DFO-B							
Parameter	Exp.	6-31G	6-31G(d)	6-31+G(d)	6-311G(d)	6-311G(d,p)	6-311+G(d)
Fe–O(C)	2.04 ^a	2.10	2.10	2.11	2.11	2.07	2.12
Fe–O(N)	1.98 ^a	1.98	1.96	1.98	1.96	1.97	1.98
Fe–O (All)	2.01 ^b	2.04	2.03	2.04	2.04	2.02	2.05
Fe–C/N (All)	2.84 ^b	2.88	2.83	2.84	2.83	2.82	2.85
C–O	1.28 ^a	1.30	1.27	1.27	1.26	1.28	1.26
N–O	1.38 ^a	1.41	1.37	1.37	1.36	1.37	1.36
N–C	1.32 ^a	1.34	1.33	1.33	1.33	1.33	1.33
O–Fe–O	78.7 ^a	77.6	77.8	77.3	77.3	77.7	76.8
Axial O–Fe–O	164.2 ^a	165.7	164.9	164.9	166.0	161.8	164.7

the solution EXAFS measurements, however, which is important because the average Fe–O bond length is a good predictor of the β factors (Domagal-Goldman and Kubicki, 2008). Each of the other predicted bond lengths were within 0.03 Å of the experimentally measured values. Axial O–Fe–O bond angles were overestimated by $<2^\circ$. Good agreement between the 6-31G(d) and 6-31+G(d) results showed that addition of diffuse functions did not significantly impact the predictions. Likewise, similarity between the 6-31G(d) and 6-311G(d) results showed that triple-versus double-zeta basis sets had a modest effect on the predictions. In terms of agreement with the experimental measurements, the most cost-effective basis set examined was 6-31G(d).

3.2. Solvation method effects: large-scale structure

The effects of solvation on the Fe(III)-DFO-B structure were also considered. Although solvation did not dramatically affect the local bonding environment surrounding the Fe atom, it did affect the overall structure of the complex. For example, when modeling the protonated (i.e., $-\text{NH}_3^+$) gas-phase complex, the amine group formed H-bonds with the oxygen atoms coordinated to the Fe atom. Despite the dramatic effects of these intramolecular H-bonds on the complex (Fig. 1), there was not a significant effect on the local bonding environment surrounding the Fe atom (Table 2).

To model the protonated structure more reliably, we used two different methods to account for solvation. In one scenario, hydration was accounted for explicitly by sur-

rounding the complex with 72 H₂O molecules (e.g., water droplet). In the second scenario, the IEFPCM (Cancès et al., 1997) method was used to implicitly account for hydration (Table 2). Differences in the predicted bond lengths for these two solvation methods were less than 0.03 Å for bonds directly involved in Fe complexation. Bond angle differences were 1.8° for the O–Fe–O angles and 6.1° for the O–Fe–O axial angles. For both of the solvated model calculations, the predicted Fe–O bond lengths exhibited better agreement with experiment compared to the gas-phase calculations described in Section 3.1.

For the solvated model calculations, major artificial changes to the Fe(III)-DFO-B complex resulting from intra-molecular H-bonding were absent, as evidenced by the relatively large distances between the amine N and Fe atoms. This distance changed by <1.5 Å between the deprotonated gas-phase model, the implicitly solvated model, and the explicitly solvated model. This difference is small compared to the ~ 4 Å decrease in the Fe–N distance that appeared in gas-phase calculations of protonated Fe-DFO-B. Agreement between the deprotonated gas-phase model and the solvated models implies that the structure of Fe-DFO-B can be reasonably approximated by gas-phase models if artificial intra-molecular H-bonding is reasonably minimized.

3.3. Chemical specificity of DFO-B for Fe(III)

In Table 3, the local bonding environment of uncomplexed DFO-B is compared with Fe(III)-, Fe(II)-, and Al(III)-DFO-B to evaluate differences that may be qualitatively related to the ligand-metal affinity. Replacing Fe(III) with Fe(II) resulted in lengthening of all the Fe–O bonds by more than 0.1 Å and a decrease in the O–Fe–O angles by 1 – 2.5° . Replacing Fe(III) with Al(III) resulted in shortening of the M–O bonds by 0.08–0.15 Å and an increase in the O–M–O angles of 3 – 4° . The effects of substituting different metals into the DFO-B complex were limited to the local bonding environment. C–O, N–O, and N–C bond length changes were smaller than their associated errors, and the overall geometry of the complex was relatively unchanged (Supplemental Fig. 1). Changes to the local bonding environment were significantly larger than differences arising from use of various basis sets, solvation methods, and disagreements between predicted and experimental structures. The relative length of the M–O bonds followed the order, Fe(II) > Fe(III) > Al(III), consistent with differences in the ionic radii of the metal cations (0.78 Å for Fe(II), 0.645 Å for Fe(III), and 0.535 Å for Al(III)). However, the shorter length of the Al(III)-DFO-B bonds was inconsistent with the preference of DFO-B for Fe(III) over Al(III). The ability of DFO-B to preferentially complex Fe(III) when Fe(III) and Al(III) are co-present in soils must therefore arise from some other factor.

The differences between the metal-oxygen bonds in Fe(III)-DFO-B and those in Fe(II)-DFO-B and Al(III)-DFO-B were revealed by NBO analysis (Table 4). NBO analysis assigns molecular orbital electron densities using a single electron projection of the full electron distribution, thus allowing the analysis of single electron orbitals

Table 2
Fe(III)-DFO-B structural data from experimental measurements (Exp.) and MO/DFT predictions. The experimental measurements are from X-ray diffraction measurements of crystalline Fe-DFO-B (a—Dhungana et al., 2001), and EXAFS measurements of Fe-DFO-B in solution (b—Edwards et al., 2005). The MO/DFT predictions correspond to deprotonated gas-phase Fe-DFO-B (DFO-B), protonated gas-phase Fe-DFO-B+ (DFO-B+), protonated Fe-DFO-B in solution using the IEFPCM method (PCM), and protonated Fe-DFO-B in solution using 72 explicit H₂O molecules (Droplet). The ‘Amine N–Fe’ distance is not an actual bond length, but represents the distance between the N in the amine functional group of DFO-B and the Fe atom. The short amine N–Fe distance in the DFO-B+ model (3.74 Å) is associated with intramolecular H-bonding that is an artifact of the model and highlights the need to take into account the effects of solvation. All values except the N–Fe distance are averaged (Å for bond lengths and ° for angles).

Fe (III)-DFO-B					
Parameter	Exp.	DFO-B	DFO-B+	PCM	Droplet
Fe–O(C)	2.04 ^a	2.11	2.14	2.08	2.07
Fe–O(N)	1.98 ^a	1.96	1.96	1.99	1.97
Fe–O (All)	2.01 ^b	2.04	2.06	2.03	2.02
Fe–C/N (All)	2.84 ^b	2.83	2.89	2.87	2.88
C–O	1.28 ^a	1.26	1.31	1.30	1.31
N–O	1.38 ^a	1.36	1.40	1.41	1.44
N–C	1.32 ^a	1.33	1.33	1.33	1.32
O–Fe–O	78.7 ^a	77.3	76.8	77.4	79.2
Axial O–Fe–O	164.2 ^a	166.0	163.7	162.0	168.1
Amine N–Fe	8.466 ^a	8.77	3.74	8.89	7.48

Table 3

MO/DFT predictions of changes to the local bonding environment of DFO-B without a metal and complexed with Fe(II), Fe(III), and Al(III). Values were averaged and standard deviations are listed in parentheses (Å for bond lengths and ° for angles). M–O bonds changed according to the size of the ionic radii of the metal (Fe(II) > Fe(III) > Al(III)), but the C–O, N–O, and N–C bonds were unchanged.

Parameter	Edwards ^a	DFO-B	Fe(II)	Fe(III)	Al(III)
M–O(C)	—	—	2.24 (0.03)	2.11 (0.02)	1.96 (0.01)
M–O(N)	—	—	2.07 (0.01)	1.97 (0.01)	1.89 (0.01)
C–O	1.24	1.23	1.26 (0.01)	1.26 (0.00)	1.27 (0.00)
N–O	1.41	1.41	1.36 (0.01)	1.36 (0.00)	1.37 (0.00)
N–C	1.36	1.36	1.33 (0.01)	1.33 (0.00)	1.32 (0.00)
O–M–O	—	—	74.8 (0.6)	77.3 (0.5)	81.5 (0.5)
Axial O–M–O	—	—	165.1 (4.3)	166.0 (1.2)	169.8 (1.1)

^a Edwards et al. (2005).

(Weinhold and Landis, 2001). In this study, NBO analysis was used for quantification of the metal cation atomic charges, the occupancy of atomic orbitals, and the atomic orbital contributions to molecular orbitals. The occupancy of natural atomic orbitals agreed with the occupancy expected for the given nuclear charges and calculated electronic charges of the metals. The natural electronic configurations determined by the NBO analysis were: [core]4s^{0.26}3d^{5.91}4p^{0.01}4d^{0.04} with a charge of +1.77 for Fe(III), [core]4s^{0.21}3d^{6.26}4p^{0.01}4d^{0.02} with a charge of +1.49 for Fe(II), and [core]3s^{0.36}3p^{0.72}3d^{0.02}4p^{0.01} with a charge of +1.88 for Al(III). This qualitatively agrees with expectations that Al(III) and Fe(III) have greater positive charges than Fe(II), and with the expected valence orbital occupancies for each metal (mostly 4s and 3d in Fe and 3s and 3p in Al). The ~6 d-electrons for Fe(III) is in agreement with experimental evidence for ligand-to-metal charge transfer between DFO-B and Fe(III) (Edwards et al., 2005).

The NBO predictions indicate that Fe(II)- and Al(III)-DFO-B bonds are completely ionic, but that four of the Fe(III)-DFO-B bonds are covalent. Table 4 shows the orbital occupancies for Fe(II)-, Fe(III)- and Al(III)-DFO-B for the metal atoms in each of these complexes and for the four O atoms that form the covalent Fe–O bonds in Fe(III)-DFO-B, labeled in Fig. 2. Fe(II)-DFO-B and Al(III)-DFO-B did not exhibit any covalent bonding between the metal and DFO-B, as evidenced by the lack of Fe–O and Al–O participation by electrons from O atoms in these complexes. This contrasts with the O atoms in the Fe(III)-DFO-B complex, for which four covalent Fe–O bonds were predicted. The presence of covalent bonding between the *sp* orbital of O and the *sd* orbital of Fe(III) may effectively result in the high chemical specificity of DFO-B for Fe(III).

3.4. IR frequencies

The predicted IR frequencies for the de-protonated gas-phase Fe(III)-DFO-B complex and protonated Fe(III)-DFO-B in solution (modeled implicitly using the IEFPCM method) reproduced the experimentally measured IR frequencies with reasonable accuracy (Table 5 and Supplemental Fig. 2, and EA-1). Theoretical spectra (Fig. 3) were generated in Gaussview (Dennington et al., 2003) by

applying peaks with a half-width of 5 cm⁻¹ to the scaled frequencies. The mean difference between the predicted gas-phase IR frequencies presented here and the experimental IR frequencies measured by Edwards et al. (2005) was 19 cm⁻¹ (average error of 1.3%, and root-mean-squared difference (RMSD) of 26 cm⁻¹). The mean difference between the IEFPCM predicted IR frequencies and experimental IR frequencies was 15 cm⁻¹ (average error of 1.2% and RMSD of 18 cm⁻¹). The accuracy of the IR frequency predictions was comparable to a previous theoretical study of an analog of DFO-B (Table 5, Edwards et al., 2005), which exhibited an average error 23 cm⁻¹ (1.5% average error and RMSD of 32 cm⁻¹).

The advantage of including solvation was more apparent when examining the best fit line through the model predictions. If the model predictions exactly reproduce the experimental measurements, then all model frequencies would fall on the line $y = x$ when plotted as a function of experimental frequencies (Supplemental Fig. 2). The best fit line for the gas-phase calculation was $y = 1.0287x - 38.97$, with an r^2 value of 0.98. The best fit line for the IEFPCM model calculation was $y = 1.0019x - 1.513$, with an r^2 value 0.99. The decrease in error associated with the IEFPCM method resulted primarily from better prediction of the C=O stretching modes. The IEFPCM calculation of the 1577 cm⁻¹ and 1627 cm⁻¹ vibrational modes were in error by 5 cm⁻¹ and 28 cm⁻¹, respectively, compared to errors of 34 cm⁻¹ and 61 cm⁻¹ for the gas-phase calculations, and 44 cm⁻¹ and 78 cm⁻¹, respectively, for calculations of a gas-phase DFO-B analog (Edwards et al., 2005). The accuracy of the models used in this study was an improvement over the predictions from aHA analogs of DFO-B. This is important for calculating equilibrium isotope constants as they depend exponentially on the predicted frequencies. However, the modest changes in the errors justify the methods employed by Edwards et al. (2005), as their methods were much less computationally demanding. Nevertheless, their study did not include Fe isotope fractionations.

The root-mean-squared error in the predicted IR frequencies from this study was 26 cm⁻¹, and the root-mean-squared error in the predicted frequencies for various Fe-organic complexes, including those from a previous study (Domagal-Goldman and Kubicki, 2008), was 31 cm⁻¹. Be-

Table 4

NBO analysis of DFO-B complexes with Fe(II), Fe(III), and Al(III). Single-point calculations were performed with the B3LYP/6-311++G(d,p) method. Orbital occupancies are shown for the metal atoms and the 4 O atoms that exhibit covalent bonding with Fe(III). By comparing the orbital occupancies of similar atoms in different complexes, the source of the electrons participating in covalent bonds can be tentatively identified. Integers next to the O atoms are strictly for labeling purposes (see Fig. 2). 2-center covalent bonds are labeled A–B, where A and B are the two atoms donating electrons to the bond. A–B* indicates an anti-bonding orbital between A and B. Lone pair valence electrons are labeled LP. LP* indicates an unoccupied lone pair orbital. Contributions from individual atomic orbitals are also listed. Note the only complex for which the metal cation has electrons in covalent bonds is Fe(III)-DFO-B.

Atom	Fe(II)			Fe(III)			Al(III)		
	Type	Occ.	Composition	Type	Occ.	Composition	Type	Occ.	Composition
O 27	O–N	0.9931	9% s _O , 40% p _O , 10% s _N , 30% p _N	O–N	0.9917	9% s _O , 42% p _O , 12% s _N , 37% p _N	O–N	0.9938	9% s _O , 42% p _O , 12% s _N , 37% p _N
	LP	0.9842	59% s, 42% p	O–Fe	0.9813	17% s _O , 70% p _O , 4% s _{Fe} , 9% d _{Fe}	LP	0.9821	36% s, 64% p
	LP	0.9211	21% s, 79% p	O–Fe	0.9530	89% p _O , 11% d _{Fe}	LP	0.9397	100% p
	LP	0.9128	3% s, 97% p	LP	0.9794	62% s, 38% p	LP	0.9094	46% s, 54% p
O 28	O–N	0.9931	9% s _O , 40% p _O , 13% s _N , 38% p _N	O–N	0.9918	9% s _O , 42% p _O , 12% s _N , 37% p _N	O–N	0.9938	9% s _O , 42% p _O , 12% s _N , 37% p _N
	LP	0.9832	61% s, 39% p	O–N	0.9429	65% p _O , 35% p _N	LP	0.9818	36% s, 64% p
	LP	0.9208	7% s, 93% p	O–N*	0.6967	35% p _O , 65% p _N	LP	0.9414	100% p
	LP	0.9134	15% s, 85% p	O–Fe	0.9817	17% s _O , 70% p _O , 4% s _{Fe} , 9% d _{Fe}	LP	0.9100	46% s, 54% p
				LP	0.9794	63% s, 37% p			
O 57	O–N*	0.9750	52% p _O , 48% p _N	O–C	0.9934	24% s _O , 41% p _O , 11% s _C , 24% p _C	O–C	0.9939	25% s _O , 40% p _O , 11% s _C , 24% p _C
	O–N	0.6130	48% p _O , 52% p _N	O–Fe	0.9640	12% s _O , 79% p _O , 3% s _{Fe} , 6% d _{Fe}	LP	0.9704	36% s, 64% p
	O–C	0.9947	25% s _O , 39% p _O , 11% s _C , 25% p _C	LP	0.9744	50% s, 50% p	LP	0.909	26% s, 74% p
	LP	0.9768	55% s, 45% p	LP	0.7985	100% p	LP	0.8352	100% p
	LP	0.9184	6% s, 94% p						
O 72	O–N	0.9935	9% s _O , 40% p _O , 13% s _N , 38% p _N	O–Fe	0.9512	87% p _O , 13% s ^{25.64} _{Fe}	O–N	0.9938	9% s _O , 42% p _O , 12% s _N , 37% p _N
	LP	0.9839	60% s, 40% p	O–N	0.9915	10% s _O , 41% p _O , 12% s _N , 37% p _N	LP	0.9819	36% s, 64% p
	LP	0.9245	13% s, 87% p	LP	0.9786	62% s, 38% p	LP	0.9399	100% p
	LP	0.9076	9% s, 91% p	LP	0.8623	18% s, 82% p	LP	0.9087	46% s, 54% p
Fe/Al	LP*	0.1241	100% d	Fe–O27	0.9813	17% s _O , 70% p _O , 4% s _{Fe} , 9% d _{Fe}	LP*	0.1780	100% s
	LP*	0.1209	100% d	Fe–O27	0.9813	89% p _O , 11% d _{Fe}	LP*	0.1232	100% p
	LP*	0.1011	98% s, 2% d	Fe–O28	0.9817	17% s _O , 70% p _O , 4% s _{Fe} , 9% d _{Fe}	LP*	0.1225	100% p
	LP*	0.0658	100% d	Fe–O57	0.9640	12% s _O , 79% p _O , 3% s _{Fe} , 6% d _{Fe}	LP*	0.1166	100% p
	LP*	0.0569	100% d	Fe–O72	0.9512	87% p _O , 13% d _{Fe}			
	LP	0.9726	100% d	LP	0.1577	100% d			

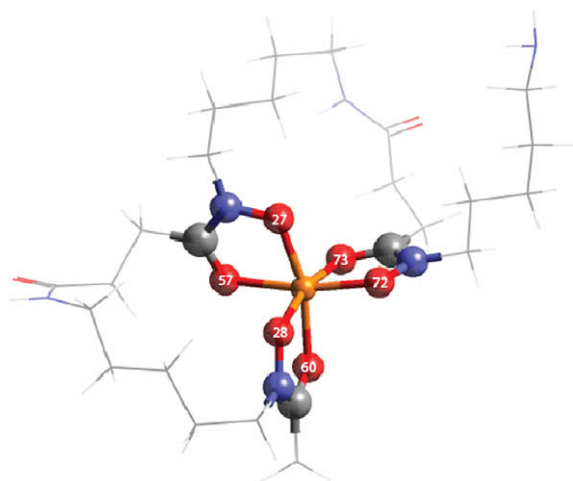


Fig. 2. Close up of the Fe–O bonds from the gas-phase, deprotonated Fe-DFO-B optimized geometry (Fig. 1b). O atoms (in red) bound to the Fe atom are labeled with numbers consistent with those listed in Table 2. The numbering is consistent across different models—Fe(II), Fe(III), and Al(III).

cause of the lack of low-frequency, isotopically-sensitive vibrational modes in the DFO-B measurements (Edwards et al., 2005), we use the latter value when evaluating the accuracy of the Fe isotope fractionation factors. The errors of the predicted IR frequencies were translated into errors in predictions of equilibrium isotope fractionation factors by randomly generating 20 errors for each predicted frequency, using a standard deviation of 31 cm^{-1} . This allowed the β factors to be re-calculated 20 times with ran-

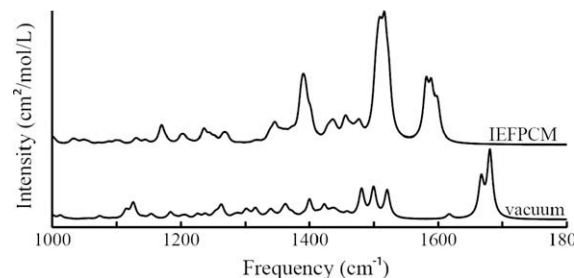


Fig. 3. Predicted IR spectra for B3LYP/6-311G(d) gas-phase calculations of Fe(III)-DFO-B (vacuum) and B3LYP/6-31G(d) IEFPCM calculations (IEFPCM). Vibrational frequencies were calculated as described in Section 2.2, and the spectra were generated from these frequencies using a full-width half-maximum of 5 cm^{-1} in Gaussview (Dennington et al., 2003).

dom errors applied to each vibrational mode. The confidence intervals reported in this study represent the standard deviations of the 20 re-calculations of β . Errors in predictions of $1000\cdot\ln(\alpha)$ were calculated by taking the square root of the sum of the squares of the $1000\cdot\ln(\beta)$ errors, and were $\sim 0.25\%$. A more detailed discussion on this and other sources of error in MO/DFT predictions of Fe isotope fractionation factors can be found in previous work (Domagal-Goldman and Kubicki, 2008).

3.5. Isotopic equilibrium in solution

Accurate prediction of the structures and IR vibrational frequencies for Fe-DFO-B complexes enabled the calculation of equilibrium isotope fractionations. $1000\cdot\ln(\beta)$ values

Table 5

Comparison of observed and calculated IR vibrational frequencies (scaled). Frequencies are listed in cm^{-1} . Intensities are listed in $\text{cm}^{-2}/\text{mol/L}$, converted from km/mol using a factor of 100 (Kubicki et al., 1993). The calculations from Edwards et al. (2005) were for an uncomplexed model, and those from this study are for the Fe(III)-DFO-B complex. The assignments listed are from IR measurements published by Edwards et al. (2005). All predicted frequencies from this study (including those that do not correlate to experimentally-determined frequencies) are listed in Electronic Annex EA-1, along with their intensities and $^{56}\nu/^{54}\nu$ ratios.

Edwards et al. (2005)			This study			
Exp.	Theoretical	Assignment	Gas-Phase	Inten.	IEFPCM	Inten.
1049	1036	$\nu\text{C-C}$ $\nu\text{C-N}$	1046	2205	1035	2010
1184	1188	$\delta\text{C-H twist}$ $\delta\text{C-H wag}$	1196	4045	1170	7672
1209	—	—	—	—	1236	6425
1355	1351	$\delta\text{C-H wag}$ $\delta\text{C-H twist}$	1324	5078	1347	3933
1374	1375	$\nu\text{C-N}$ $\delta\text{C-H wag}$ $\delta\text{C-H rock}$ $\delta\text{C-H twist}$	1380	2806	1390	20273
1421	1427	$\delta\text{CCN bend}$ $\delta\text{CCC bend}$	1418	4221	1428	4969
1453	1486	$\delta\text{NOH bend}$ $\nu\text{C-N rock}$ $\nu\text{C-N rock}$	1449	5642	1477	7276
1577	1621	$\nu\text{C=O}$	1543	23114	1582	32335
1627	1705	$\nu\text{C=O}$ $\nu\text{C-N}$	1688	45111	1599	10789

have been predicted for both Fe(II) and Fe(III) coordinated with H₂O (Jarzecki et al., 2004; Anbar et al., 2005), complexed by oxalate and catecholate (Domagal-Goldman and Kubicki, 2008), and now complexed by DFO-B (Table 6 and Fig. 4). Equilibrium Fe isotope fractionations can thus be predicted for these different Fe species in solution (see Eq. (2)) by taking the differences of their $1000 \cdot \ln(\beta)$ values (i.e., by calculating the $1000 \cdot \ln(\alpha)$ values for the reaction in question).

We predict an equilibrium fractionation of $-0.34 \pm 0.25\text{‰}$ between Fe(III)-DFO-B and Fe(III)-(H₂O)₆ at 22 °C (Table 6), in disagreement with the $+0.60 \pm 0.15\text{‰}$ value measured by Dideriksen et al. (2008) between Fe(III)-DFO-B and inorganic phases (primarily composed of Fe(III)-(H₂O)₆). If the experimental measurements are accurate within reported uncertainties, either the model predictions of the $1000 \cdot \ln(\beta)$ values for the organic fraction are too large or the model predictions of the $1000 \cdot \ln(\beta)$ values for the inorganic fraction are too small (or both, with some combination of the two sources of error).

Previous predictions of $1000 \cdot \ln(\alpha)$ values for equilibrium between inorganic solution and mineral phases (Domagal-Goldman and Kubicki, 2008) also differ from experimental measurements by $\sim 1.0\text{‰}$, with the predictions of aqueous phase $1000 \cdot \ln(\beta)$ values too large compared to mineral phase values. Thus, the discrepancies with experiment in both theoretical studies could be caused by overestimates of aqueous phase inorganic $1000 \cdot \ln(\beta)$. This could be due, in part, to not accounting for all inorganic phases present in an experiment. To test this possibility, we calculated the $1000 \cdot \ln(\beta)$ values of Fe(III)-(H₂O)₅(OH), a major component of inorganic Fe(III) in experiments, and of Fe(III)₂-(H₂O)₁₀(OH)₂, an Fe-dimer complex (Fig. 5) that is stoichiometrically equivalent to Fe(III)-(H₂O)₅(OH) and may be the structure that exists in solution. The predicted $1000 \cdot \ln(\alpha)$ value for the Fe-dimer complex at 22 °C was 8.20 ± 0.12 . This value leads to a prediction of $+0.45 \pm 0.23$ for isotopic equilibrium between Fe(III)-DFO-B and Fe(III)₂-(H₂O)₆(OH)₂, within experimental er-

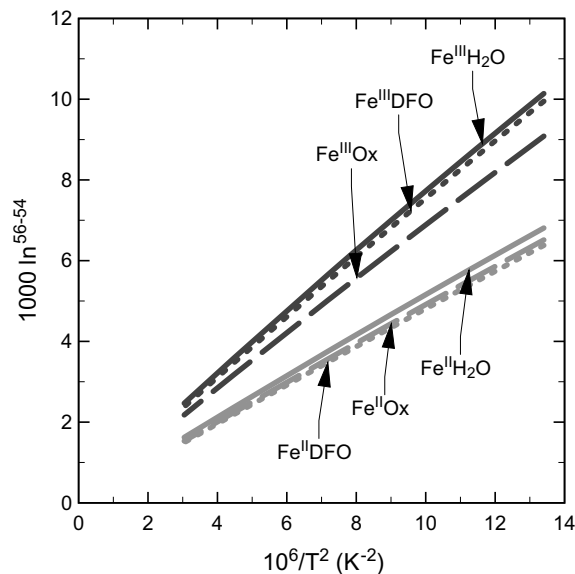


Fig. 4. $1000 \cdot \ln(\beta)$ values plotted against $1/T^2$ (10^6 K^{-2}). $^{56}\text{Fe}/^{54}\text{Fe}$ increases towards the top of the figure, and temperature increases towards the left side of the figure. Note the separation between Fe³⁺ and Fe²⁺ phases, which indicates the importance of redox reactions in isotopic fractionations. Values for Fe-(H₂O)₆ and Fe-(oxalate)₃ are from Domagal-Goldman and Kubicki (2008).

ror of the isotopic equilibrium between Fe(III)-DFO-B and inorganic precipitates. This agreement may suggest that fractionation is controlled by isotopic equilibrium between Fe(III)-DFO-B and Fe(III)₂-(H₂O)₁₀(OH)₂ prior to precipitation of inorganic Fe(III).

Given the degree to which equilibrium between Fe(III)-DFO-B and *all* inorganic phases was obtained in the experiments, and the short timescales of precipitation, it is unlikely that equilibrium between Fe(III)-DFO-B and a single inorganic phase is responsible for the measured fractionation. A better approach would be to weigh the $1000 \cdot \ln(\beta)$

Table 6

Predicted $1000 \cdot \ln(\beta)$ values for Fe(III) complexed with water, oxalate, catecholate, hydroxide, and DFO-B. These calculations used the UB3LYP/6-311G(d,p) methodology, IEFPCM to handle solvation effects, and a frequency scale factor of 0.956.

T (°C)	$\text{Fe}^{\text{III}}(\text{H}_2\text{O})_6^{3+}$	$\text{Fe}^{\text{III}}(\text{OH})(\text{H}_2\text{O})_5^{2+}$	$(\text{Fe}^{\text{III}})_2(\text{OH})_2(\text{H}_2\text{O})_6^{2+}$	$\text{Fe}^{\text{III}}\text{DFOB}^+$	$\text{Fe}^{\text{III}}(\text{Ox})_3^{3-}$	$\text{Fe}^{\text{III}}(\text{Cat})_3^{3-}$
0	9.98 ± 0.18	10.19 ± 0.18	9.48 ± 0.14	9.62 ± 0.22	9.09 ± 0.18	8.84 ± 0.25
10	9.34 ± 0.17	9.54 ± 0.17	8.86 ± 0.13	8.99 ± 0.21	8.50 ± 0.17	8.26 ± 0.23
20	8.76 ± 0.16	8.96 ± 0.16	8.31 ± 0.12	8.42 ± 0.20	7.96 ± 0.16	7.73 ± 0.22
22	8.65 ± 0.16	8.84 ± 0.16	8.20 ± 0.12	8.31 ± 0.20	7.86 ± 0.16	7.63 ± 0.22
25	8.49 ± 0.16	8.68 ± 0.15	8.05 ± 0.12	8.15 ± 0.19	7.71 ± 0.16	7.49 ± 0.21
30	8.23 ± 0.15	8.42 ± 0.15	7.80 ± 0.12	7.90 ± 0.18	7.47 ± 0.15	7.26 ± 0.21
40	7.74 ± 0.15	7.93 ± 0.14	7.34 ± 0.11	7.43 ± 0.17	7.02 ± 0.14	6.82 ± 0.19
50	7.30 ± 0.14	7.48 ± 0.13	6.92 ± 0.11	7.00 ± 0.16	6.61 ± 0.13	6.42 ± 0.18
60	6.89 ± 0.13	7.07 ± 0.13	6.53 ± 0.10	6.60 ± 0.15	6.24 ± 0.13	6.06 ± 0.17
70	6.52 ± 0.13	6.69 ± 0.12	6.17 ± 0.09	6.24 ± 0.15	5.90 ± 0.12	5.72 ± 0.16
80	6.17 ± 0.12	6.34 ± 0.11	5.84 ± 0.09	5.90 ± 0.14	5.58 ± 0.11	5.41 ± 0.16
90	5.85 ± 0.11	6.02 ± 0.11	5.54 ± 0.09	5.59 ± 0.13	5.29 ± 0.11	5.13 ± 0.15
100	5.56 ± 0.11	5.72 ± 0.10	5.26 ± 0.08	5.31 ± 0.13	5.02 ± 0.10	4.87 ± 0.14
200	3.52 ± 0.07	3.63 ± 0.07	3.33 ± 0.05	3.35 ± 0.08	3.17 ± 0.07	3.07 ± 0.09
300	2.42 ± 0.05	2.51 ± 0.05	2.29 ± 0.05	2.30 ± 0.06	2.18 ± 0.05	2.11 ± 0.09

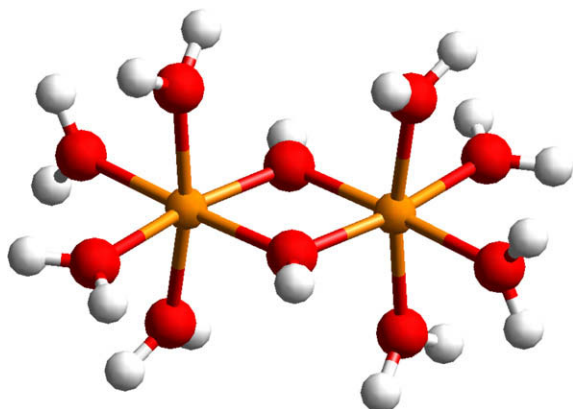


Fig. 5. Structure of $\text{Fe(III)}_2\text{(OH)}_2\text{(H}_2\text{O)}_5$, as predicted by B3LYP/6-311G(d,p) utilizing IEFPCM to model solvation effects. Orange atoms represent Fe(III), red atoms represent O, and white atoms represent H. This is a potential structure for Fe(III) in solution, and may help describe the measured equilibrium isotope fractionation between inorganically bound Fe and Fe bound to organic ligands. (For interpretation of the references to colour in this figure legend, the reader is referred to the web version of this paper.)

values of the inorganic phases by their reported abundances based upon the results of thermodynamic modeling. The abundances in the experiment were 70% $\text{Fe(III)-(H}_2\text{O)}_6$ ($1000\cdot\ln(\beta) = 8.65 \pm 0.16$), 29% $\text{Fe(III)}_2\text{(H}_2\text{O)}_8\text{(OH)}_2$, ($1000\cdot\ln(\beta) = 8.20 \pm 0.12$), and 1% $\text{Fe(II)-(H}_2\text{O)}_6$, ($1000\cdot\ln(\beta) = 5.66 \pm 0.16$). Thus, the predicted $1000\cdot\ln(\beta)$ value for the inorganic phase is $0.70 \times 8.65 + 0.29 \times 8.20 + 0.01 \times 5.66 = 8.46$, leading to a Fe(III)-DFO-B-Fe-inorganic fractionation prediction of $-0.15 \pm 0.24\text{‰}$. This represents an improvement over the predictions based solely on $\text{Fe(III)-(H}_2\text{O)}_6$, but is not within error of the experimental measurement, indicating that either isotopic equilibrium in experiments is dominated by isotopic exchange between Fe(III)-DFO-B and $\text{Fe(III)}_2\text{(H}_2\text{O)}_{10}\text{(OH)}_2$ prior to precipitation of Fe-oxyhydroxides, or there is some other source of error in predicted or measured $1000\cdot\ln(\alpha)$ values.

The predicted equilibrium fractionations between Fe(III)-DFO-B and $\text{Fe(III)-(oxalate)}_3$ ($+0.45 \pm 0.25\text{‰}$, Table 6) and between Fe(III)-DFO-B and $\text{Fe(III)-(catecholate)}_3$ ($+0.68 \pm 0.25\text{‰}$, Table 6) were close to differences between the isotopic composition of Fe in cells and Fe remaining in solution during hornblende dissolution, measured to be $+0.85$ and $+1.17 \pm 0.20\text{‰}$ (Brantley et al., 2001). This agreement is consistent with isotopic equilibrium between Fe complexed with small organic ligands and Fe complexed with DFO-B and no isotopic fractionation between Fe(III)-DFO-B and cell material. While other fractionations may exist in such a system, including reactions inside cells and during transfer of Fe from siderophores to the cell, the fractionation reported by Brantley et al. (2001) can be explained by the predicted equilibrium fractionations between Fe complexed to small organic ligands and Fe complexed to siderophores.

Experiments have shown that the rate at which Fe is leached from mineral surfaces increases when DFO-B is co-present with oxalate (Cheah et al., 2003). This implies that

Fe sequestration occurs through a multi-step process: Fe is first leached by small organic ligands, complexed by siderophores in solution, and delivered to cells via Fe–siderophore complexes. Our results support this conceptual model because the predicted equilibrium Fe isotope fractionation between Fe(III)-DFO-B and $\text{Fe(III)-(oxalate)}_3$ matches the experimental differences between the isotopic compositions of cells and solution during hornblende dissolution (Brantley et al., 2001). Such agreement is consistent with delivery of Fe to cells exclusively via Fe(III)-DFO-B complexes. Fractionations have also been shown to exist during dissolution of minerals (Brantley et al., 2001, 2004; Wiederhold et al., 2006) and during precipitation of Fe(III) phases (Welch et al., 2003). Thus, there may be at least three sources of fractionation during biological uptake of Fe: dissolution of the initial mineral phase by small organic acids, equilibrium between various Fe-ligand complexes in solution, and re-precipitation of inorganic mineral phases.

4. CONCLUSIONS

The prediction of isotope fractionation factors, placed in the context of experimental measurements, further develops a molecular-scale understanding of the transport of Fe from minerals to bacterial cells. Small organic acids remove Fe from the mineral surface, and then Fe is complexed by siderophores that ultimately transport the Fe to bacterial cells. This conceptual model is supported by our explanation of previous measurements of a fractionation between Fe in solution and Fe in bacterial cells during the leaching of Fe from hornblende (Brantley et al., 2001). The explanation of these data is based on our predicted fractionation factor for isotopic equilibrium between Fe(III)-DFO-B and either $\text{Fe(III)-(catecholate)}_3$ or $\text{Fe(III)-(oxalate)}_3$.

The role of siderophores in this process is to prevent Fe precipitation by efficiently sequestering it in Fe-organic complexes. This is only possible because of the chemical specificity siderophores have for Fe(III), which NBO analysis suggests is the result of covalent metal-oxygen bonds that are absent in Al(III)-DFO-B and Fe(II)-DFO-B . In Fe(III)-DFO-B, the Fe(III)-O bonding orbitals are fully populated. These orbitals allow siderophores to efficiently sequester Fe and not other metals, thereby giving siderophores a unique and important role in biological Fe acquisition.

ACKNOWLEDGMENTS

The work of J.D.K. and S.D.G. was supported of an ACS Petroleum Research Fund grant: Experimental and Theoretical Investigation on Adsorption of Extracellular Compounds onto Mineral Surfaces. Computational support at Penn State was provided by the Center for Environmental Kinetics Analysis (CEKA), an NSF/DOE Environmental Molecular Sciences Institute and by the Center for Materials Simulation (CEMS), a PSU MRSEC facility. Support for K.W.P. and D.L.S. and computational resources at the University of Delaware were provided by Delaware EPSCoR through the Delaware Biotechnology Institute with funds from the National Science Foundation Grant EPS-0447610 and the State of Delaware. We thank the reviewers of this manuscript, including

C. Johnson, V. Polyakov, E. Schauble, and an anonymous reviewer; as would like to thank the anonymous reviewers of an earlier version of our work.

APPENDIX A. SUPPLEMENTARY DATA

Supplementary data associated with this article can be found, in the online version, at doi:10.1016/j.gca.2008.09.031.

REFERENCES

- Accelrys (2003) *Cerius² Modeling Environment*. Accelrys, Inc., San Diego.
- Albrecht-Gary A. M. and Crumbliss A. L. (1998) Coordination chemistry of siderophores: thermodynamics and kinetics of iron chelation and release. In *Metal Ions in Biological Systems* (eds. H. Sigel and A. Sigel). M. Dekker, New York.
- Anbar A. D., Jarzecki A. A. and Spiro T. G. (2005) Theoretical investigation of iron isotope fractionation between $\text{Fe}(\text{H}_2\text{O})_6^{3+}$ and $\text{Fe}(\text{H}_2\text{O})_6^{2+}$: implications for iron stable isotope geochemistry. *Geochim. Cosmochim. Acta* **69**, 825–837.
- Anderegg G., Leplatte F. and Schwarzenbach G. (1963) Hydroxamatkomplexe. 3. Eisen(III)-austausch zwischen sideraminen und komplexen—diskussion der bildungskonstanten der hydroxamatkomplexe. *Helvet. Chim. Acta* **46**, 1409–1422.
- Becke A. D. (1997) Density-functional thermochemistry. 5. Systematic optimization of exchange-correlation functionals. *J. Chem. Phys.* **107**, 8554–8560.
- Borgias B., Hugi A. D. and Raymond K. N. (1989) Isomerization and solution structures of desferrioxamine-B complexes of Al^{3+} and Ga^{3+} . *Inorg. Chem.* **28**(18), 3538–3545.
- Boukhalfa H. and Crumbliss A. L. (2002) Chemical aspects of siderophore mediated iron transport. *Biometals* **15**, 325–339.
- Brantley S. L., Liermann L. and Bullen T. D. (2001) Fractionation of Fe isotopes by soil microbes and organic acids. *Geology* **29**, 535–538.
- Brantley S. L., Liermann L. J., Guynn R. L., Anbar A., Icopini G. A. and Barling J. (2004) Fe isotopic fractionation during mineral dissolution with and without bacteria. *Geochim. Cosmochim. Acta* **68**, 3189–3204.
- Cancès E., Mennucci B. and Tomasi J. (1997) A new integral equation formalism for the polarizable continuum model: theoretical background and applications to isotropic and anisotropic dielectrics. *J. Chem. Phys.* **107**, 3032–3041.
- Carpenter J. E. and Weinhold F. (1988) Analysis of the geometry of the hydroxymethyl radical by the different hybrids for different spins Natural Bond Orbital procedure. *Theochem—J. Mol. Struct.* **46**, 41–62.
- Cheah S. F., Kraemer S. M., Cervini-Silva J. and Sposito G. (2003) Steady-state dissolution kinetics of goethite in the presence of desferrioxamine B and oxalate ligands: implications for the microbial acquisition of iron. *Chem. Geol.* **198**, 63–75.
- Cundari T. R. and Stevens W. J. (1993) Effective core potential methods for the lanthanides. *J. Chem. Phys.* **98**, 5555–5565.
- Dennington, II, R., Keith T., Millam J., Eppinnett K., Hovell W. L. and Gilliland R. (2003) *GaussView*. Semichem, Inc., Shawnee Mission, KS.
- Dhungana S., White P. S. and Crumbliss A. L. (2001) Crystal structure of ferrioxamine B: a comparative analysis and implications for molecular recognition. *J. Biol. Inorg. Chem.* **6**, 810–818.
- Dideriksen K., Baker J. A. and Stipp S. L. S. (2008) Equilibrium Fe isotope fractionation between inorganic aqueous Fe(III) and the siderophore complex, Fe(III)-desferrioxamine B. *Earth Planet. Sci. Lett.* **269**(1–2), 280–290.
- Domagal-Goldman S. D. and Kubicki J. D. (2008) Density functional theory predictions of equilibrium isotope fractionation of iron due to redox changes and organic complexation. *Geochim. Cosmochim. Acta* **72**(21), 5201–5216.
- Edwards D. C. and Myneni S. C. B. (2005) Hard and soft X-ray absorption spectroscopic investigation of aqueous Fe(III)-hydroxamate siderophore complexes. *J. Phys. Chem. A* **109**, 10249–10256.
- Edwards D. C., Nielsen S. B., Jarzecki A. A., Spiro T. G. and Myneni S. C. B. (2005) Experimental and theoretical vibrational spectroscopy studies of acetohydroxamic acid and desferrioxamine B in aqueous solution: effects of pH and iron complexation. *Geochim. Cosmochim. Acta* **69**, 3237–3248.
- Evers A., Hancock R. D., Martell A. E. and Motekaitis R. J. (1989) Metal-ion recognition in ligands with negatively charged oxygen donor groups—complexation of Fe(III), Ga(III), In(III), Al(III), and other highly charged metal-ions. *Inorg. Chem.* **28**, 2189–2195.
- Foster J. P. and Weinhold F. (1980) Natural hybrid orbitals. *J. Am. Chem. Soc.* **102**, 7211–7218.
- Frisch M. J., Trucks G. W., Schlegel H. B., Scuseria G. E., Robb M. A., Cheeseman J. R., Montgomery Jr. J. A., Vreven T., Kudin K. N., Burant J. C., Millam J. M., Iyengar S. S., Tomasi J., Barone V., Mennucci B., Cossi M., Scalmani G., Rega N., Petersson G. A., Nakatsuji H., Hada M., Ehara M., Toyota K., Fukuda R., Hasegawa J., Ishida M., Nakajima T., Honda Y., Kitao O., Nakai H., Klene M., Li X., Knox J. E., Hratchian H. P., Cross J. B., Bakken V., Adamo C., Jaramillo J., Gomperts R., Stratmann R. E., Yazyev O., Austin A. J., Cammi R., Pomelli C., Ochterski J. W., Ayala P. Y., Morokuma K., Voth G. A., Salvador P., Dannenberg J. J., Zakrzewski V. G., Dapprich S., Daniels A. D., Strain M. C., Farkas O., Malick D. K., Rabuck A. D., Raghavachari K., Foresman J. B., Ortiz J. V., Cui Q., Baboul A. G., Clifford S., Cioslowski J., Stefanov B. B., Liu G., Liashenko A., Piskorz P., Komaromi I., Martin R. L., Fox D. J., Keith T., Al-Laham M. A., Peng C. Y., Nanayakkara A., Challacombe M., Gill P.M.W., Johnson B., Chen W., Wong M. W., Gonzalez C. and Pople J. A., 2004. Gaussian 03, Revision C.02. CT, Wallingford.
- Hehre W. J., Radom L., Schleyer P. V. and Pople J. (1985) *Ab Initio Molecular Orbital Theory*. John Wiley & Sons, New York.
- Hernlem B. J., Vane L. M. and Sayles G. D. (1996) Stability constants for complexes of the siderophore desferrioxamine B with selected heavy metal cations. *Inorg. Chim. Acta* **244**, 179–184.
- Holmen B. A. and Casey W. H. (1996) Hydroxamate ligands, surface chemistry, and the mechanism of ligand-promoted dissolution of goethite $\alpha\text{-FeOOH(s)}$. *Geochim. Cosmochim. Acta* **60**(22), 4403–4416.
- Holmen B. A., Tejedor-Tejedor M. I. and Casey W. H. (1997) Hydroxamate complexes in solution and at the goethite-water interface: a cylindrical internal reflection Fourier transform infrared spectroscopy study. *Langmuir* **13**(8), 2197–2206.
- Jarzecki A. A., Anbar A. D. and Spiro T. G. (2004) DFT analysis of $\text{Fe}(\text{H}_2\text{O})_6^{3+}$ and $\text{Fe}(\text{H}_2\text{O})_6^{2+}$ structure and vibrations; implications for isotope fractionation. *J. Phys. Chem. A* **108**, 2726–2732.
- Johnson C., Skulan J. A., Beard B. L., Sun H., Nealson K. H. and Braterman P. S. (2002) Isotopic fractionation between Fe(III) and Fe(II) in aqueous solutions. *Earth Planet. Sci. Lett.* **195**, 141–153.
- Kiss T. and Farkas E. (1998) Metal-binding ability of desferrioxamine B. *J. Inclusion Phenomena Mol. Recogn. Chem.* **32**, 385–403.
- Koch W. and Holthausen M. C. (2001) *A Chemist's Guide to Density Functional Theory*, second ed. Wiley-VCH, New York.

- Kochian L. V. (1995) Cellular mechanisms of aluminum toxicity and resistance in plants. *Annu. Rev. Plant Physiol. Plant Mol. Biol.* **46**, 237–260.
- Kubicki J. D., Sykes D. and Rossman G. R. (1993) Calculated trends of OH infrared stretching vibrations with composition and structure in aluminosilicate molecules. *Phys. Chem. Miner.* **20**, 425–432.
- Kurzak B., Kozłowski H. and Farkas E. (1992) Hydroxamic and aminohydroxamic acids and their complexes with metal-ions. *Coord. Chem. Rev.* **114**, 169–200.
- Lee C. T., Yang W. T. and Parr R. G. (1988) Development of the Colle–Salvetti correlation-energy formula into a functional of the electron-density. *Phys. Rev. B* **37**, 785–789.
- Leong J. and Raymond N. (1975) Coordination isomers of biological iron transport compounds. 4. Geometrical isomers of chromic desferrioxamine-B. *J. Am. Chem. Soc.* **97**(2), 293–296.
- Martin J. H. and Fitzwater S. E. (1988) Iron deficiency limits phytoplankton growth in the north-east Pacific subarctic. *Nature* **331**, 341–343.
- Redlich O. (1935) A general relationship between the oscillation frequency of isotropic molecules—(with remarks on the calculation of harmonious force constants). *Zeitschrift Fur Physikalische Chemie-Abteilung B-Chemie Der Elementarprozesse Aufbau Der Materie* **28**, 371–382.
- Reed A. E., Curtiss L. A. and Weinhold F. (1988) Intermolecular interactions from a Natural Bond Orbital, donor–acceptor viewpoint. *Chem. Rev.* **88**, 899–926.
- Reed A. E. and Weinhold F. (1983) Natural bond orbital analysis of near-Hartree–Fock water dimer. *J. Chem. Phys.* **78**, 4066–4073.
- Reed A. E., Weinstock R. B. and Weinhold F. (1985) Natural-population analysis. *J. Chem. Phys.* **83**, 735–746.
- Schaad L. (1999) Ab initio test of the usefulness of the Redlich–Teller product rule in computing kinetic isotope effects. *Can. J. Chem.* **77**, 875–878.
- Stephens P. J., Devlin F. J., Chabalowski C. F. and Frisch M. J. (1994) Ab-initio calculation of vibrational absorption and circular-dichroism spectra using density-functional force-fields. *J. Phys. Chem.* **98**, 11623–11627.
- Urey H. C. (1947) The thermodynamic properties of isotopic substances. *J. Chem. Soc.*, 562–581.
- Walker J. C. G., Klein C., Schidlowski M., Schopf J. W., Stevenson D. J. and Walter M. R. (1983) Environmental evolution of the Archean-early Proterozoic Earth. In *Earliest Biosphere: Its Origin and Evolution Princeton, Earth's* (ed. J. W. Schopf). University Press, Princeton.
- Weinhold F. and Landis C. R. (2001) Natural bond orbitals and extensions of localized bonding concepts. *Chemistry Education: Research and Practice in Europe* **2**, 91–104.
- Welch S. A., Beard B. L., Johnson C. M. and Braterman P. S. (2003) Kinetic and equilibrium Fe isotope fractionation between aqueous Fe(II) and Fe(III). *Geochim. Cosmochim. Acta* **67**, 4231–4250.
- Wiederhold J. G., Kraemer S. M., Teutsch N., Borer P. M., Halliday A. N. and Kretzschmar R. (2006) Iron isotope fractionation during proton-promoted, ligand-controlled, and reductive dissolution of goethite. *Environ. Sci. Technol.* **40**, 3787–3793.

Associate Editor: Clark M. Johnson